Published in final edited form as:
Clin Exp Metastasis. 2008 ; 25(7): 799–810. doi:10.1007/s10585-008-9193-z.

Reactive glia are recruited by highly proliferative brain metastases of breast cancer and promote tumor cell colonization

Daniel P. Fitzgerald, **Diane Palmieri**, **Emily Hua**, **Elizabeth Hargrave**, and **Patricia S. Steeg**
Women's Cancers Section, Laboratory of Molecular Pharmacology, National Cancer Institute, Building 37, Room 1126, National Institutes of Health, Bethesda, MD 20892, USA

Jeanne M. Herring, **Yongzhen Qian**, and **Eleazar Vega-Valle**
Laboratory Animal Sciences Program, Science Applications International Corporation-Frederick, National Cancer Institute NIH, Frederick, MD, USA

Robert J. Weil
Department of Neurosurgery and Neurological Institute, Brain Tumor & Neuro-Oncology Center, Cleveland Clinic, Cleveland, OH, USA

Andreas M. Stark
Department of Neurosurgery, Schleswig-Holstein University Medical Center, Campus Kiel, Germany

Alexander O. Vortmeyer
Surgical Neurology Branch, National Institute of Neurological Disorders and Stroke NIH, Bethesda, MD, USA

Abstract

Interactions between tumor cells and the microenvironment are crucial to tumor formation and metastasis. The central nervous system serves as a “sanctuary” site for metastasis, resulting in poor prognosis in diagnosed patients. The incidence of brain metastasis is increasing; however, little is known about interactions between the brain and metastatic cells. Brain pathology was examined in an experimental model system of brain metastasis, using a subline of MDA-MB-231 human breast cancer cells. The results were compared with an analysis of sixteen resected human brain metastases of breast cancer. Experimental metastases formed preferentially in specific brain regions, with a distribution similar to clinical cases. In both the 231-BR model, and in human specimens, Ki67 expression indicated that metastases were highly proliferative (~50%). Little apoptosis was observed in either set of tumors. In the model system, metastases elicited a brain inflammatory response, with extensive reactive gliosis surrounding metastases. Similarly, large numbers of glial cells were found within the inner tumor mass of human brain metastases. In vitro co-cultures demonstrated that glia induced a ~5-fold increase in metastatic cell proliferation ($P < 0.001$), suggesting that brain tissue secretes factors conducive to tumor cell growth. Molecules used to signal between tumor cells and the surrounding glia could provide a new avenue of therapeutic targets for brain metastases.

Correspondence to: Daniel P. Fitzgerald.
e-mail: fitzgeda@mail.nih.gov.

Keywords

Brain metastasis; Brain pathology; Breast cancer; Neuroinflammation; Reactive glia; Xenograft

Introduction

Greater than 100,000 cancer patients each year, in the United States alone, develop brain metastases [1]. The prognosis of these patients is dismal, with ~80% mortality within 1 year of diagnosis [2]. While melanoma has the greatest propensity to form secondary lesions in the brain, the higher incidence of breast and lung cancers make these tumors the most common origin of brain metastases [1]. Brain metastases are thought to be hematogenous in origin, and most breast cancer patients present visceral metastases prior to the formation of brain lesions [1,2]. Traditionally, only 10-16% of metastatic breast cancer patients developed brain metastases. The incidence appears to be increasing, however, especially among Her-2^+ and triple-negative subsets [3,4]. This is likely the result, at least in part, of the development of therapeutic agents which successfully treat visceral, but not brain metastases. Thus, the brain becomes a “sanctuary” site for metastases.

Therapeutic intervention for brain metastatic disease is extremely limited. Radiation therapy, both stereotactic and whole brain, is the most common treatment. There is a significant impact on the quality of life for many patients [1,5,6]. Surgical resection, with or without accompanying whole brain radiation, is also performed. The blood brain barrier poses a significant obstacle in delivering most drugs into the brain [7]. As a result, chemotherapy has rarely been used to treat brain metastases. However, significant effort is being made to identify drugs which either disrupt or penetrate the blood-brain barrier [5,7-9].

Xenograft model systems of brain metastasis have been developed [10-18]. Four models specific to breast cancer brain metastasis have been described, with preferential metastasis to the brain by hematogenous spread. Rye, et al. [19] described isolation of metastatic cells from the bone marrow of a patient with grade-II invasive lobular carcinoma. Two of the model systems [12,17], developed in parallel, used in vivo passage in the mouse to select highly brain metastatic derivative lines of human MDA-MB-231 breast cancer cells. The MDA-MB-231-Parental cell line was originally isolated from a pleural effusion. A fourth model system has recently been described [10]. These four model systems have provided insight into the molecular events associated with progression to brain metastasis, as well as serving as models for potential therapeutics. Kim et al. [12] demonstrated that brain metastatic cells upregulated expression of Vascular Endothelial Growth Factor (VEGF) expression, and that a VEGF inhibitor retarded growth of brain metastases in their “MDA-231 BR3” model system. Chen et al. [10] showed that adaptation of their “BCM2” cell line to the brain was associated with changes in cell metabolism, including enhanced mitochondrial respiration. Using the “231-BR” xenograft model system, we have reported increased brain metastatic potential upon overexpression of the Human Epidermal Growth Factor-2 receptor, Her-2 [3]. Furthermore, the Her-2 inhibitor Lapatanib retarded growth of brain metastases, suggesting some efficacy of this agent in preventing brain metastases [20]. To date, work on the model systems has primarily focused on changes intrinsic to the metastatic cancer cells. Little is known about interactions and effects that the metastatic cancer cells have on the surrounding brain.

More than 100 years ago, Paget proposed a “seed and soil” hypothesis to explain the propensity of tumors to metastasize to specific organs despite hematogenous spread of tumor cells throughout the body [21]. Since then, numerous studies have demonstrated that interactions between cancer cells and the surrounding microenvironment are crucial to tumor

growth [22-26]. The success of a number of new therapeutic agents in the treatment of multiple myeloma, underscores the importance of these tumor-microenvironment interactions [27,28].

The brain may provide a particularly unique microenvironment. The extracellular matrix of the brain, although still poorly characterized, is very different from the viscera. It has a structural organization mainly based on the linear polysaccharide hyaluronan and chondroitin sulfate proteoglycans [29,30]. The blood brain barrier tightly regulates traffic into the brain parenchyma. Tight junctions between vascular endothelial cells, close association with brain astrocytes and pericytes, and high expression of protein efflux pumps, create a vasculature unlike any other in the body [7,31]. This barrier also creates an immune privileged environment. Normal brain has very few lymphocytes [32]. The brain has its own population of macrophage-like cells, called microglia, which are thought to populate the brain prior to birth [33]. In response to brain injury, these cells, along with other resident glial cells, including those of the astrocytic lineage, become activated, resulting in a "reactive glial" response. These cells become hypertrophic and motile, and infiltrate the site of injury to form a glial scar [33,34]. Numerous studies have shown that gene expression in reactive glial cells is very different from normal brain [35-40]. Even in their "resting state", astrocytes, oligodendrocytes, and microglia function as much more than a scaffold, associating with neurons to promote their survival and activity, as well as helping maintain the blood brain barrier [41,42].

In this manuscript we provide an analysis of the 231-BR xenograft model for brain metastasis of breast cancer. We report that tumor cells colonize in meninges, ventricles, and throughout the brain parenchyma, but show high incidence in specific brain regions. Metastases in all brain regions are highly proliferative with little apoptosis. Metastatic colonization is accompanied by an extensive response in the surrounding brain tissue, recruiting large numbers of reactive glia. Glial cells secrete factors which significantly increase the growth potential of the 231-BR metastatic cells in vitro, suggesting that the reactive brain may potentiate metastatic colonization in vivo. Finally, we compare these data to a cohort of surgically resected human brain metastases of breast cancer and establish that these trends also exist in clinical cases.

Materials and methods

Human metastatic brain tissue

Samples were coded with no patient identifiers and approved by the National Cancer Institute (NCI) Office of Human Subjects Research. Diagnosis and histopathologic characteristics were confirmed by a single pathologist before use in the study. Unfixed tissue samples were flash frozen in O.C.T. compound (Tissue-Tek). 5 μM frozen sections were prepared on Superfrost/Plus slides using a Shandon Cryotome FE cryostat. For immunofluorescent analysis, cut sections were fixed in 4% paraformaldehyde in Phosphate Buffered Saline (PBS pH ~ 7.4) for 15 min.

Cell culture

Production of an EGFP expressing variant of the highly brain metastatic breast cancer cell line, MDA-MB-231-Brain (231-BR), was described previously [3]. These, and all cells used in this study, were maintained in culture in Dulbecco's Modified Eagle's Medium (DMEM) plus 10% Fetal Bovine Serum (FBS), in 5% CO_2. MRC5 human lung fibroblasts were obtained from The American Type Culture Collection (ATCC). Mixed glial cell cultures were prepared from the forebrains of postnatal day 1-3 C57/Bl6 mouse pups. Forebrains

were digested briefly in 0.25% trypsin, and cells seeded and maintained in DMEM +10% FBS.

Mouse model of brain metastasis

Animal experiments were conducted under an approved Animal Use Agreement with the NCI. Under isoflurane/O_2 anesthesia, 5- to 7-week-old female BALB/c nude or NIH nu/nu mice (Charles River Laboratories) were inoculated with 10,000-175,000 cells in 0.1 ml PBS in the left cardiac ventricle. Mice were euthanized under CO_2 asphyxiation after 4-5 weeks, which correlated with the onset of neurological symptoms. Subsets of these mice were perfused with PBS followed by 4% paraformaldehyde, for optimal fixation of brain tissue, prior to surgical excision of the brain. Brains were bisected along the sagittal plane, and the right hemisphere fixed in 4% paraformaldehyde for 24 to 48 h at 4°C, transferred to 20% sucrose overnight at 4°C, and then flash frozen in OCT. Cryosections (5-10 μM thick) were serially cut and processed for histology and immunofluorescence analyses.

Histological and immunofluorescence analyses

Double-stains were performed using standard protocols with Eosin Y Solution and Mayer's Hematoxylin Solution (H&E) from Sigma Aldrich. For immunofluorescence analyses, sections were pre-blocked in PBS containing 2% FBS, 2% Goat Serum, and 0.2% TritonX-100 for several hours. Antibody incubations and all washes were carried out using this solution at room temperature. Sections were incubated for 1-2 h with primary antibody diluted 1:10-1:200. The following antibodies were used: rabbit polyclonal anti-Cleaved Caspase 3 (Cell Signaling Technology); rat anti-mouse CD11b (Chemicon); rat anti-mouse CD45 (Chemicon); mouse anti-human CD68 clone KP1 (DakoCytomation); mouse anti-human cytokeratin clone MNF116 (DakoCytomation); mouse anti-human mitochondria clone MTC02 (Thermo Scientific); rabbit polyclonal anti-pan cytokeratin (Zymed laboratories); rabbit anti-cow Glial Fibrillary Acidic Protein (DakoCytomation); rabbit monoclonal anti-Ki67 (Vector Laboratories); and rabbit polyclonal anti-(C-terminus) Neurofilament M (Chemicon). Secondary antibodies used were goat-anti-mouse and goat-anti-rabbit IgG antibodies conjugated to Alexa488 and Alexa546 (Molecular Probes), diluted 1:500, as above, for 1-2 h. Mouse antibodies used in non-perfused brains were directly conjugated to the Alexa488 Zenon reagent (Molecular Probes). Nuclei were visualized by the addition of 200 μg/ml DAPI nucleic acid stain (4′, 6-diamidino-2-phenylindole, dilactate, Molecular Probes) to the secondary antibody mixture. Sections were mounted in Fluorescent Mounting Medium (DakoCytomation), and photographed using a Zeiss Axioskop mot plus microscope with an Axiocam digital camera and Openlab software.

Analysis of tumor distribution in the mouse brain

Ten sagittal sections, spaced every 300 μM, were cut through one hemisphere of each mouse brain and stained with H&E. The locations of hematoxylin-bright clusters of metastatic growth were identified by bright-field observation using a 5× objective lens.

Soft agar colonization assays

Ten thousand metastatic cells (MDA-MB-231 [231-Parental] or the brain metastatic derivative 231-BR) were plated in 2 ml of DMEM +10% FBS, with the addition of 0.3% (w/v) Bactoagar, over a 2 ml layer of 0.7% bottom agar. For co-culture experiments, 20,000 mixed glial cells, or 20,000 MRC5 lung fibroblast cells, were added to the 2 ml top agar. After 14 days in culture, colonies (>50 μm diameter) were counted under low magnification using a Nikon Eclipse TE2000-U inverted microscope. Images were captured using a Nikon Digital DXM1200 Camera with ACT-1 software. Results are representative of three (MRC5 co-culture) or five (glia co-culture) independent experiments, each performed in triplicate.

One-way Analysis of Variance (ANOVA) was performed on data sets using InStat version 3.0a for Macintosh (GraphPad Software), and yielded a significance of $P < 0.0001$ for difference between 231-BR alone versus co-culture with glia and between 231-BR versus 231-Parental.

Results

Distribution and growth of brain metastases in the 231-BR xenograft model

Isolation of the MDA-MB-231 derivative line 231-BR by repeated in vivo selection was previously reported [17]. Magnetic Resonance Imaging of injected cells revealed that they distributed rapidly throughout the brain vasculature, but that the majority (>80%) of these cells disappeared in the first few days post-injection [43]. The exceptional tumor cells which survived formed metastases throughout the parenchyma (Fig. 1a and b). Meningeal (Fig. 1c) and ventricular (Fig. 1d) metastases were also observed at a high frequency. In most experiments 175,000 231-BR cells were injected. At this cell dose, numerous metastases populated the parenchyma. Mice were necropsied approximately 23-28 days post-injection, when neurologic symptoms were often apparent. Most of the metastatic growth manifested as clusters of micrometastases which appeared to be growing along blood vessels. Larger (>50 μm^2) solid masses of metastatic growth, expanding away from the vasculature, were observed at a much lower frequencies (~3%). Introduction of fewer cells (10,000-40,000) allowed us to prolong the period of metastatic growth to 5 weeks before the onset of neurologic symptoms. At this point, numerous larger parenchymal metastases were apparent (Fig. 1b).

We asked whether experimental metastases developed in all regions of the brain, or preferentially in specific areas. Sagittal step sections through one hemisphere of 20 mouse brains were analyzed to determine the locations of metastases in the brain (Fig. 2). Metastases were found in all regions of the brain; however, the distribution of metastases was non-random. Metastases were invariably found in the cerebral cortex. The most common site of metastasis (100% of mice) was the frontal region of the cerebral cortex, frequently in the area of the olfactory cortex. The second most frequent site was the parietal/temporal cortex (95% of mice), most often found immediately dorsal to the hippocampal formation. Metastases were also almost always found in the hippocampus (90% of mice); and the medulla oblongata (90% of cases), most often in the dorsal medulla in the area of the 4th ventricle. In contrast, metastatic tumors were under-represented in more ventral structures of the forebrain, especially in basal ganglia (only 15% of mice), and the hypothalamus (only 20% of mice), and metastases in these regions were typically smaller.

Many metastatic clusters appeared along grey-white matter junctions. Moreover, metastases in all regions of the brain appeared more likely to be found near ventricles, and were often associated with metastatic growth in the ventricles. This was especially true around the 3rd ventricle, in the thalamus and midbrain, as well as in the hippocampus and visual cortex. The most common sites of ventricular metastases were in the 3rd ventricle beneath the hippocampus (60% of mice), and in the 4th ventricle between the cerebellum and medulla oblongata (60% of mice). Meningeal metastases could be found in 65% of the mice. Common sites for meningeal metastases were the ventral brain between the hypothalamus and pons; in association with the olfactory cortex; and dorsal to the midbrain and cerebellum.

Cell proliferation and cell death in mouse brains with 231-BR metastases

We performed immunofluorescence analysis with anti-Ki67 and anti-Cleaved Caspase-3 antibodies, commonly used markers for cell proliferation and for apoptotic cell death,

respectively (Fig. 3). Enhanced Green Fluorescent Protein (EGFP) expressing 231-BR tumor cells were co-stained with an anti-pan cytokeratin antibody (clone MNF116) for easy identification (green in Figs. 3, 4, and 5) in the mouse brain, although clusters of human tumor cells could also be differentiated from mouse brain cells based on the size and appearance of their nuclei stained with DAPI (blue in Figs. 3, 4, and 5). As expected, cycling cells were exceptional in normal adult mouse brain. Although metastasis results in an extensive brain injury response (see below), only a very small percentage of the brain cells surrounding the metastases entered the cell cycle. In contrast, there was a high rate of proliferation in brain metastases in the 231-BR mouse model (average = 53% cycling cells [3540/6789 cells in six mice]) (Fig. 3a and b). There was no difference in the rate of proliferation in micrometastases versus clinical (>50 μm^2 in 10 lm cut sections) parenchymal metastases (Fig. 3a) or meningeal metastases (Fig. 3b). Moreover, there was no apparent difference in proliferation of metastases in different brain regions (data not shown).

Apoptotic cells were almost never seen (n = 15 mice) in either metastatic tumor cells, or in the surrounding mouse brain (Fig. 3d). It should be noted that, in the 231-BR xenograft model (4-5 weeks), tumors with necrotic cores were rarely seen.

In order to determine whether the 231-BR model was representative of human brain metastases of breast cancer, a group of 16 surgically-excised brain metastases from breast cancer patients were analyzed. Frozen sections were prepared and stained with the same markers for comparison. Comparably high rates of proliferation were seen among cytokeratin-positive carcinoma cells in the human tumors derived from ductal-breast tissue (Fig. 3c; see also Fig. 5), ranging from 28-59% with an average of ~47% (Table 1). Although cell death was observed in the clinical samples, it was largely confined to necrotic areas (top and lower left areas in Fig. 3e, also see Fig. 5) with a low frequency of apoptosis among cytokeratin-positive tumor cells (Fig. 3e).

The mouse brain responds to the presence of 231-BR metastases with extensive reactive gliosis

To determine whether 231-BR tumor cells altered the brain microenvironment, we performed immunofluorescent staining for common markers of major cells types in the brain. Multiple sections in a minimum of five mice were examined for each marker, representative images are shown in Fig. 4. Markers used included: Neurofilament-M, expressed in the mature neurons of the adult brain (red in Fig. 4a); and Glial Fibrillary Acidic Protein (GFAP), which is expressed in astrocytes, and is particularly high in motile, hypertrophic reactive astrocytes in injured brain tissue (red in Fig. 4b-d, and h). Brain sections were also double-stained with CD11b and CD45, which are expressed in microglia, the brain macrophage (red in Fig. 4e-g). It should be noted that blood-derived monocytes would also be recognized with the CD11b/CD45 antibodies. In all cases, the metastatic carcinoma cells in the mouse brains were identified by expression of EGFP and by co-stain with anti-pan-cytokeratin or an anti-human mitochondrial antibody (green). Cell nuclei were counterstained with DAPI (blue).

In co-stains with Neurofilament-M, metastases in all brain regions were generally separated from neurons by edema (Fig. 4a). However, in co-stains with GFAP and CD11b/CD45, tumor cells were found in close contact with glial cells. As expected, only a small percentage of the mature, resting astrocytes in the normal adult brain showed a high level of GFAP expression (Fig. 4b). In contrast, a high level of GFAP was induced in reactive glia for a wide radius around the metastases (Fig. 4c), showing an extensive brain injury response. We analyzed mouse brains at an earlier time point, 14 days after introduction of the metastatic breast cancer cells. At this point the breast cancer cells are in an early stage of colonization and only small metastases are evident. GFAP-positive reactive glia are already

evident at this early time point, and are localized to the area of metastasis (Fig. 4d). Reactive astrocytes were often seen in direct contact with tumor cells, along the border of the tumor mass (Fig. 4h). Astrocytes close to the tumor cells were often hypertrophic and less dendritic relative to more distal astrocytes.

Most resting microglia in normal mouse brain show a low-level of staining with the markers CD11b and CD 45, although some increased staining is apparent near ventricles (Fig. 4e). Increased CD11b/CD45 staining around metastatic tumors suggest that reactive microglia, in addition to reactive astrocytes, were present (Fig. 4f). Microglia were in direct contact with tumor cells along the border of the tumors (Fig. 4g). Moreover, CD11b/CD45-positive cells were often seen infiltrating the inner tumor mass. Cells in or near metastases often appeared phagocytic, whereas more distant CD11b/CD45-positive cells were typically dendritic/arboreal in appearance (compare Fig. 4g to inset in Fig. 4e).

Brain metastases from breast cancer patients contain significant masses of glial cells inside the tumors

We compared the mouse model to sixteen surgical samples from human breast cancer patients. The same anti-GFAP antibody was used to examine the interaction of astrocytes with metastatic carcinoma cells in the human brain (red in Fig. 5b, c, e, j, and l). We used CD68 as a marker for human microglia/macrophages (red in Fig. 5f). The breast-derived carcinoma cells, which stain intensely with hematoxylin in Fig. 5a, d, i, and k, were identified with the same anti-pan cytokeratin antibody (green in Fig. 5b, c, e, g, h, j, and l), or a similar rabbit anti-pan cytokeratin antibody (green in Fig. 5f), which showed the same specificity. The results are summarized in Table 1. Not surprisingly, reactive astrocytes expressing high levels of GFAP (Fig. 5b) were found along the borders of the metastatic tumors (14 of 16 examined). An H&E stain of the same region is shown in Fig. 5a.

We also found islands of astrocytes in the interior of most of the tumors examined (12 of 16 metastases; Fig. 5c and e, j, and l). CD68-positive microglia/macrophages co-localized to these areas (Fig. 5f), which were cytokeratin-negative, and could be identified as separate from necrotic areas (Fig. 5h). Moreover, the morphology of the nuclei, as seen with DAPI, or hematoxylin staining, was noticeably different in the islands of glia, with much smaller nuclei than was seen in the cytokeratin-positive tumor cells. The glia often appeared in large islands or fingers (6 of 12 samples), between large fingers of cytokeratin-positive carcinoma cells (Fig. 5d and e), although some tumors (4 of 12 samples) had smaller ribbons of glial cells (Fig. 5i and j). Thus, gross morphology of the tumors appeared similar to the larger parenchymal tumors in the mouse model (compare to Fig. 1b). Metastases from patients with lobular (Fig. 5k and l) and a patient with inflammatory (not shown) breast cancer also contained a large number of glial cells within the tumor mass. Again, similar to the 231-BR mouse model, very few dividing (Fig. 5g) or apoptotic (Fig. 5h) cells were seen among GFAP-positive cells, either at the border, or in islands of glia inside the tumors. The data establish a close interaction of brain metastatic tumor cells with reactive glial cells in both an experimental xenograft model and human samples.

Mouse glial cells stimulate the anchorage independent growth of human breast cancer cells

Anchorage independent growth of cancer cell lines, seeded in soft agar, has been reported to correlate with their ability to form visceral metastases in vivo. The 231-BR cells maintain the ability to grow in soft agar (Fig. 6a), however, as has been reported for other cell lines selected for preferential metastasis to brain [44], they grow more poorly than related cell lines which preferentially metastasize to viscera, such as the highly lung metastatic 231-Parental cells (Fig. 6b). A mixed population of glial cells, derived from normal mouse brain,

will not grow in soft agar (Fig. 6d). However, when grown in co-culture, brain glial cells elicited a strong increase (4.8-fold increase, 95% confidence interval 2.77-6.85-fold, $n = 5$ experiments) in the anchorage-independent growth of the 231-BR metastatic cells (Fig. 6c). MRC5 lung fibroblasts, in contrast, did not elicit a significant increase in 231-BR cell colonization (Fig. 6f). Neither glia nor fibroblasts appeared to affect the number of colonies formed by the already robust 231-Parental breast cancer cell line. Results of typical experiments are quantified in Fig. 6e.

Discussion

This report provides the first in depth analysis of the pathology of a model system for brain metastasis of breast cancer. The data obtained from the xenograft model was compared to a set of sixteen resected human brain metastases of breast cancer. The 231-BR xenograft model shared a number of similarities with brain metastases from breast cancer patients, including proliferative and apoptotic rates, and the presence of an inflammatory microenvironment. As such, the model system may provide insight into brain metastatic progression, especially at the early stages of growth, before metastases are detectable in human patients. Moreover, the data support the hypothesis that breast cancer cells alter the brain microenvironment, and that this altered environment contributes to metastatic progression.

In the xenograft model, metastases appeared to form preferentially in specific regions of the brain. Metastases were most commonly found in the frontal and parietal cortex, and in dorsal medulla oblongata. Moreover, extensive growth was commonly found in the vicinity of the hippocampus and along the ventricles. Studies of the distribution of brain metastases of mixed origins, collected from either computed tomographic (CT) scans or magnetic resonance imaging (in a total of 388 patients between two different studies), reported a similar pattern, with the highest incidence in frontal and parietal lobes of the cortex, a much lower incidence in deeper tissues, and frequent lesions along white-grey matter junctions [45,46].

The brain responds to traumatic brain injury with a reactive glial, or “neuroinflammatory” response. Mobilized glia of multiple lineages, including astrocytes and microglia, are recruited to the injured site to form a glial scar [33,34,47]. Reactive glia are radically different from cells in the resting state [35-40]. Brain injury models in rodents reveal a complex story of interactions between reactive glia and neurons [34,42,48]. The glia can provide both stimulatory and inhibitory signals, promoting neuronal survival, and either stimulating or inhibiting the growth of neuronal cell processes in the injured area. As has been reported for surgical specimens [49], 231-BR metastatic tumors do not appear to stimulate proliferation in the surrounding mouse brain. However, in the xenograft model we observed an extensive reactive glial response in and around even small perivascular metastases. Analogous to the role of altered fibroblasts and activated inflammatory cells in primary breast tumors, it is quite possible that the reactive glia create an altered brain microenvironment which is more permissive to tumor growth/invasion. An analysis of large, surgically-resected metastases from the brains of human patients revealed significant masses of glial cells trapped within the inner-tumor mass. The existence of these glial islands within, as well as surrounding the metastases, provides the possibility of glial-tumor cell interactions throughout metastatic progression.

Our in vitro results demonstrate that glial cells secrete factors which may promote metastatic growth. Both resting and activated glia provide a host of factors which contribute to neuronal survival, and could potentially be co-opted by tumor cells to provide a similar support function. There is already a long list of candidate factors, known to be produced by

glial cells, which could affect tumor growth. These include glial cell line-derived neurotrophic factor, sphingosine-1-phosphate, chemokine CXC motif ligand 12, transforming growth factor-α and β, interleukins, insulin like growth factor, autotaxin, heparin-binding epidermal growth factor, hepatocyte growth factor and scatter factor, chemokine CXC motif ligand 12, epidermal growth factor, pleiotrophin, hepatocyte growth factor and scatter factor, heparinase, and matrix metalloproteinases [24,50-52]. However, rodent models suggest that reactive glia can have very different effects on the surrounding tissue, depending on the context [48]. Metastatic tumor cells could potentially alter the glia in a novel way, resulting in a unique interaction. Comparisons of gene/protein expression patterns of parenchymal tissue from normal, injured, and metastatic brain may reveal this "conversation" between tumor and glia. Similar to recent breakthroughs in the treatment of cancers in the bone [27], such information could provide a whole new avenue of molecular targets for therapeutic agents against brain metastasis.

Acknowledgments

We would like to thank Hong Wang (Developmental Neurobiology Section of the NHLBI Division of Intramural Research, NIH) for providing mixed glial cultures used in the soft agar experiments. This research was supported by the US Department of Defense Breast Cancer Research Program, grant number: W81 XWH-062-0033; and the Intramural Research Program of the National Cancer Institute, CCR, NIH.

Abbreviations

DAPI 4′6	Diamidino-2-phenylindole
EGFP	Enhanced Green Fluorescent Protein
GFAP	Glial Fibrillary Acidic Protein
H&E	Hematoxylin and eosin

References

1. Weil RJ, Palmieri DC, Bronder JL, et al. Breast cancer metastasis to the central nervous system. Am J Pathol 2005;167(4):913–920. [PubMed: 16192626]
2. Palmieri D, Smith QR, Lockman PR, et al. Brain metastases of breast cancer. Breast Dis 2006;26:139–147. [PubMed: 17473372]
3. Palmieri D, Bronder JL, Herring JM, et al. Her-2 overexpression increases the metastatic outgrowth of breast cancer cells in the brain. Cancer Res 2007;67(9):4190–4198. doi: 10.1158/0008-5472.CAN-06-3316. [PubMed: 17483330]
4. Santarelli JG, Sarkissian V, Hou LC, et al. Molecular events of brain metastasis. Neurosurg Focus 2007;22(3):E1. doi:10.3171/foc.2007.22.3.2. [PubMed: 17608351]
5. Cavaliere R, Schiff D. Chemotherapy and cerebral metastases: Misperception or reality? Neurosurg Focus 2007;22(3):E6. doi:10.3171/foc.2007.22.3.7. [PubMed: 17608359]
6. Chang EL, Lo S. Diagnosis and management of central nervous system metastases from breast cancer. Oncologist 2003;8(5):398–410. doi:10.1634/theoncologist.8-5-398. [PubMed: 14530493]
7. Neuwelt EA. Mechanisms of disease: the blood-brain barrier. Neurosurgery 2004;54(1):131–140. doi:10.1227/01.NEU.0000 097715.11966.8E Discussion 41-2. [PubMed: 14683550]
8. van den Bent MJ, Hegi ME, Stupp R. Recent developments in the use of chemotherapy in brain tumours. Eur J Cancer 2006;42(5):582–588. doi:10.1016/j.ejca.2005.06.031. [PubMed: 16427778]
9. Drappatz J, Wen PY. Chemotherapy and targeted molecular therapies for brain metastases. Expert Rev Neurother 2006;6(10):1465–1479. doi:10.1586/14737175.6.10.1465. [PubMed: 17078787]
10. Chen EI, Hewel J, Krueger JS, et al. Adaptation of energy metabolism in breast cancer brain metastases. Cancer Res 2007;67(4):1472–1486. doi:10.1158/0008-5472.CAN-06-3137. [PubMed: 17308085]

11. Fidler IJ, Schackert G, Zhang RD, et al. The biology of melanoma brain metastasis. Cancer Metastasis Rev 1999;18(3):387–400. doi:10.1023/A:1006329410433. [PubMed: 10721492]
12. Kim LS, Huang S, Lu W, et al. Vascular endothelial growth factor expression promotes the growth of breast cancer brain metastases in nude mice. Clin Exp Metastasis 2004;21(2):107–118. doi: 10.1023/B:CLIN.0000024761.00373.55. [PubMed: 15168728]
13. Kusters B, Leenders WP, Wesseling P, et al. Vascular endothelial growth factor-a(165) induces progression of melanoma brain metastases without induction of sprouting angiogenesis. Cancer Res 2002;62(2):341–345. [PubMed: 11809675]
14. Lu W, Bucana CD, Schroit AJ. Pathogenesis and vascular integrity of breast cancer brain metastasis. Int J Cancer 2007;120(5):1023–1026. doi:10.1002/ijc.22388. [PubMed: 17187362]
15. Saito N, Hatori T, Murata N, et al. A double three-step theory of brain metastasis in mice: The role of the pia mater and matrix metalloproteinases. Neuropathol Appl Neurobiol 2007;33(3):288–298. doi:10.1111/j.1365-2990.2007.00799.x. [PubMed: 17493010]
16. Schackert G, Price JE, Zhang RD, et al. Regional growth of different human melanomas as metastases in the brain of nude mice. Am J Pathol 1990;136(1):95–102. [PubMed: 2297053]
17. Yoneda T, Williams PJ, Hiraga T, et al. A bone-seeking clone exhibits different biological properties from the mda-mb-231 parental human breast cancer cells and a brain-seeking clone in vivo and in vitro. J Bone Miner Res 2001;16(8):1486–1495. doi: 10.1359/jbmr.2001.16.8.1486. [PubMed: 11499871]
18. Mendes O, Kim HT, Stoica G. Expression of mmp2, mmp9 and mmp3 in breast cancer brain metastasis in a rat model. Clin Exp Metastasis 2005;22(3):237–246. doi:10.1007/s10585-005-8115-6. [PubMed: 16158251]
19. Rye PD, Norum L, Olsen DR, et al. Brain metastasis model in athymic nude mice using a novel muc1-secreting human breast-cancer cell line, ma11. Int J Cancer 1996;68(5):682–687. doi : 10.1002/(SICI)1097-0215(19961127)68:5<682::AID-IJC20>3.0.CO;2-2. [PubMed: 8938153]
20. Gril B, Palmieri D, Bronder JL, Herring JM, Vega-Valle E, Feigenbaum L, et al. Effect of lapatinib on the outgrowth of metastatic breast cancer cells to the brain. Journal of the National Cancer Institute. in press.
21. Paget S. Distribution of secondary growths in cancer of the breast. Lancet 1889;1:571–573. doi: 10.1016/S0140-6736(00)49915-0.
22. Bhowmick NA, Moses HL. Tumor-stroma interactions. Curr Opin Genet Dev 2005;15(1):97–101. doi:10.1016/j.gde.2004.12.003. [PubMed: 15661539]
23. De Wever O, Mareel M. Role of tissue stroma in cancer cell invasion. J Pathol 2003;200(4):429–447. doi:10.1002/path.1398. [PubMed: 12845611]
24. Hoelzinger DB, Demuth T, Berens ME. Autocrine factors that sustain glioma invasion and paracrine biology in the brain microenvironment. J Natl Cancer Inst 2007;99(21):1583–1593. doi: 10.1093/jnci/djm187. [PubMed: 17971532]
25. Li H, Fan X, Houghton J. Tumor microenvironment: the role of the tumor stroma in cancer. J Cell Biochem 2007;101(4):805–815. doi:10.1002/jcb.21159. [PubMed: 17226777]
26. Schedin P, O'Brien J, Rudolph M, et al. Microenvironment of the involuting mammary gland mediates mammary cancer progression. J Mammary Gland Biol Neoplasia 2007;12(1):71–82. doi: 10.1007/s10911-007-9039-3. [PubMed: 17318269]
27. Anderson KC. Targeted therapy of multiple myeloma based upon tumor-microenvironmental interactions. Exp Hematol 2007;35(4 Suppl 1):155–162. doi:10.1016/j.exphem.2007.01.024. [PubMed: 17379101]
28. Hideshima T, Mitsiades C, Tonon G, et al. Understanding multiple myeloma pathogenesis in the bone marrow to identify new therapeutic targets. Nat Rev Cancer 2007;7(8):585–598. doi: 10.1038/nrc2189. [PubMed: 17646864]
29. Novak U, Kaye AH. Extracellular matrix and the brain: components and function. J Clin Neurosci 2000;7(4):280–290. doi: 10.1054/jocn.1999.0212. [PubMed: 10938601]
30. Rauch U. Extracellular matrix components associated with remodeling processes in brain. Cell Mol Life Sci 2004;61(16):2031–2045. doi:10.1007/s00018-004-4043-x. [PubMed: 15316653]

31. de Vries NA, Beijnen JH, Boogerd W, et al. Blood-brain barrier and chemotherapeutic treatment of brain tumors. Expert Rev Neurother 2006;6(8):1199–1209. doi:10.1586/14737175.6.8.1199. [PubMed: 16893347]
32. Engelhardt B. Molecular mechanisms involved in t cell migration across the blood-brain barrier. J Neural Transm 2006;113(4):477–485. doi:10.1007/s00702-005-0409-y. [PubMed: 16550326]
33. Streit WJ, Conde JR, Fendrick SE, et al. Role of microglia in the central nervous system's immune response. Neurol Res 2005;27(7):685–691. [PubMed: 16197805]
34. Sofroniew MV. Reactive astrocytes in neural repair and protection. Neuroscientist 2005;11(5): 400–407. doi:10.1177/10738584 05278321. [PubMed: 16151042]
35. Kobori N, Clifton GL, Dash P. Altered expression of novel genes in the cerebral cortex following experimental brain injury. Brain Res Mol Brain Res 2002;104(2):148–158. doi:10.1016/S0169-328X(02)00331-5. [PubMed: 12225869]
36. Long Y, Zou L, Liu H, et al. Altered expression of randomly selected genes in mouse hippocampus after traumatic brain injury. J Neurosci Res 2003;71(5):710–720. doi:10.1002/jnr.10524. [PubMed: 12584729]
37. Matzilevich DA, Rall JM, Moore AN, et al. High-density microarray analysis of hippocampal gene expression following experimental brain injury. J Neurosci Res 2002;67(5):646–663. doi: 10.1002/jnr.10157. [PubMed: 11891777]
38. Natale JE, Ahmed F, Cernak I, et al. Gene expression profile changes are commonly modulated across models and species after traumatic brain injury. J Neurotrauma 2003;20(10):907–927. doi: 10.1089/089771503770195777. [PubMed: 14588109]
39. Raghavendra Rao VL, Dhodda VK, Song G, et al. Traumatic brain injury-induced acute gene expression changes in rat cerebral cortex identified by genechip analysis. J Neurosci Res 2003;71(2):208–219. doi:10.1002/jnr.10486. [PubMed: 12503083]
40. Sun L, Lee J, Fine HA. Neuronally expressed stem cell factor induces neural stem cell migration to areas of brain injury. J Clin Invest 2004;113(9):1364–1374. [PubMed: 15124028]
41. Bezzi P, Volterra A. A neuron-glia signalling network in the active brain. Curr Opin Neurobiol 2001;11(3):387–394. doi:10.1016/S0959-4388(00)00223-3. [PubMed: 11399439]
42. Giaume C, Kirchhoff F, Matute C, et al. Glia: the fulcrum of brain diseases. Cell Death Differ 2007;14(7):1324–1335. doi:10.1038/sj.cdd.4402144. [PubMed: 17431421]
43. Heyn C, Ronald JA, Ramadan SS, et al. In vivo mri of cancer cell fate at the single-cell level in a mouse model of breast cancer metastasis to the brain. Magn Reson Med 2006;56(5):1001–1010. doi:10.1002/mrm.21029. [PubMed: 17029229]
44. Zhang RD, Fidler IJ, Price JE. Relative malignant potential of human breast carcinoma cell lines established from pleural effusions and a brain metastasis. Invasion Metastasis 1991;11(4):204–215. [PubMed: 1765433]
45. Delattre JY, Krol G, Thaler HT, et al. Distribution of brain metastases. Arch Neurol 1988;45(7): 741–744. [PubMed: 3390029]
46. Hwang TL, Close TP, Grego JM, et al. Predilection of brain metastasis in gray and white matter junction and vascular border zones. Cancer 1996;77(8):1551–1555. doi :10.1002/(SICI)1097-0142(19960415)77:8<1551::AID-CNCR19>3.0.CO;2-Z. [PubMed: 8608542]
47. Busch SA, Silver J. The role of extracellular matrix in cns regeneration. Curr Opin Neurobiol 2007;17(1):120–127. doi:10.1016/j.conb.2006.09.004. [PubMed: 17223033]
48. Ajtai BM, Kalman M. Reactive glia support and guide axon growth in the rat thalamus during the first postnatal week. A sharply timed transition from permissive to non-permissive stage. Int J Dev Neurosci 2001;19(6):589–597. doi:10.1016/S0736-5748(01) 00038-7. [PubMed: 11600320]
49. Colodner KJ, Montana RA, Anthony DC, et al. Proliferative potential of human astrocytes. J Neuropathol Exp Neurol 2005;64(2):163–169. [PubMed: 15751231]
50. Graeber MB, Scheithauer BW, Kreutzberg GW. Microglia in brain tumors. Glia 2002;40(2):252–259. doi:10.1002/glia.10147. [PubMed: 12379912]
51. Nuttall RK, Silva C, Hader W, et al. Metalloproteinases are enriched in microglia compared with leukocytes and they regulate cytokine levels in activated microglia. Glia 2007;55(5):516–526. doi: 10.1002/glia.20478. [PubMed: 17216595]

52. Nishizuka I, Ishikawa T, Hamaguchi Y, et al. Analysis of gene expression involved in brain metastasis from breast cancer using cdna microarray. Breast Cancer (Tokyo, Japan) 2002;9(1):26–32.

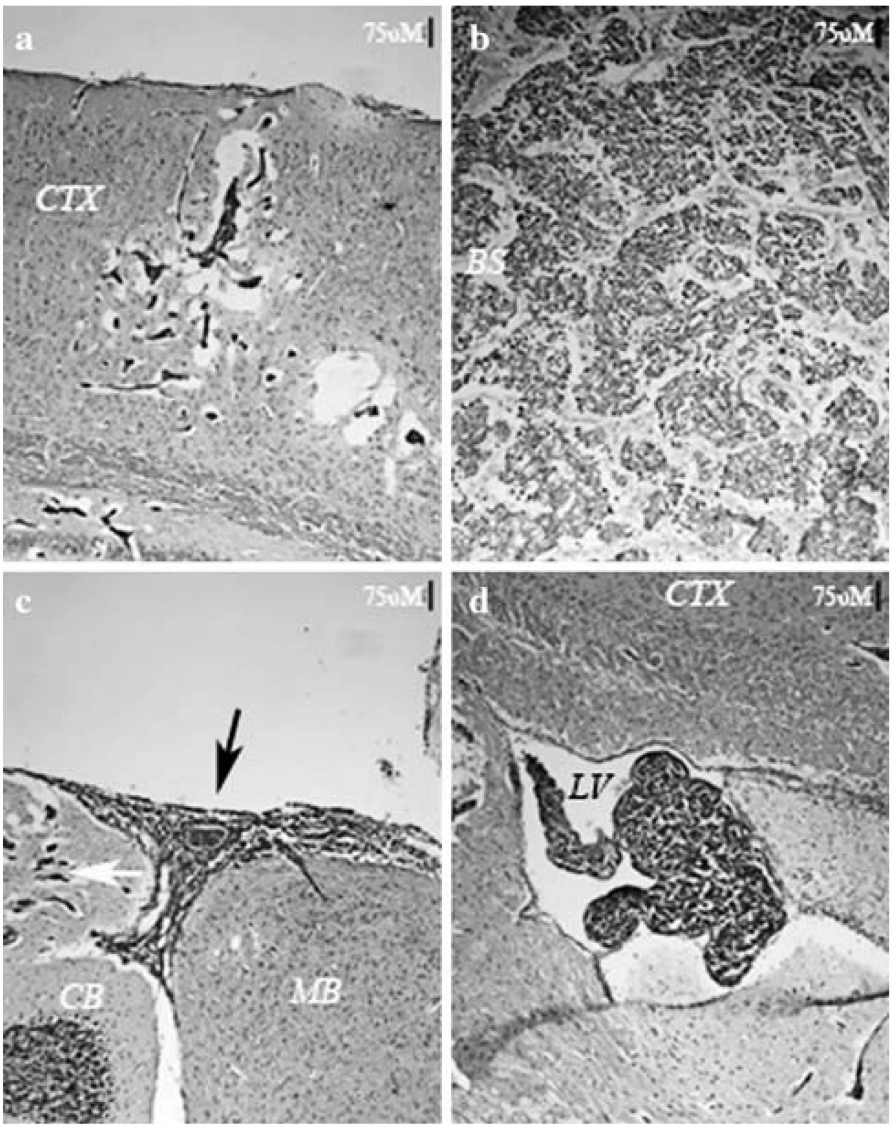

Fig. 1.

Metastatic colonization in the mouse brain by 231-BR breast cancer cells. (**a**) Four weeks after intracardiac injection of metastatic breast cancer cells into a mouse host, the majority of metastatic growth manifests as clusters of micrometastases, which can be found throughout the brain parenchyma. In (**a**), metastases in the cerebral cortex are visible as hematoxylin-positive cells, separated by edema from the surrounding brain tissue. (**b**) After five weeks, larger metastases are evident, which appear to have coalesced into single tumors. (**c**) and (**d**) At four weeks, large metastases are found in the meningeal space (black arrow in **c**), and in the ventricles (**d**), suggesting the 231-BR metastatic tumor cells grow readily in cerebral spinal fluid. Micrometastases in the cerebellum (white arrow) are also visible in (**c**). All sections were prepared from mouse brain frozen in O.C.T., stained with H&E, and photographed with a 10× objective. Scale bars indicate 75 micrometers. BS = brain stem; CB = cerebellum; CTX = cerebral cortex; LV = lateral ventricle; MB = midbrain

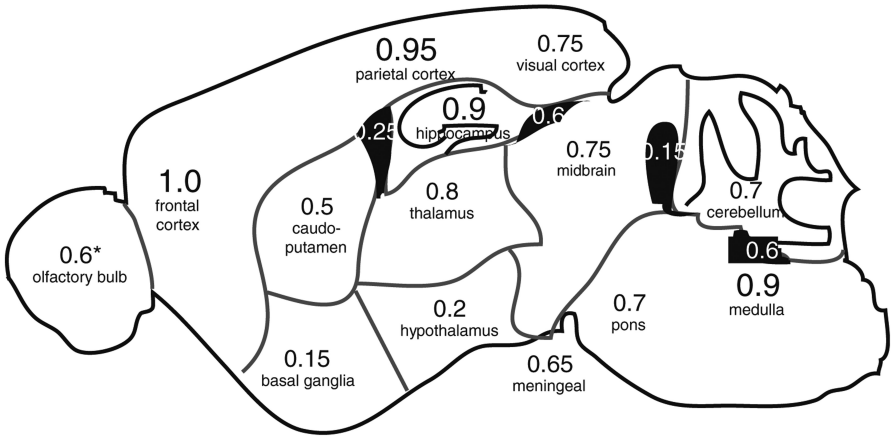

Fig. 2.

Distribution of 231-BR metastases in the mouse brain. Four to five weeks after introduction of 231-BR cells, sagittal cryosections were prepared across one hemisphere of the mouse brain, stained with H&E, and scored for the locations of metastatic tumors. Numbers shown represent the frequency among 20 mice (*15 with olfactory bulbs attached), in which metastatic growth was found in a given region of the brain. Numbers in white show the frequency of metastases in ventricles. The frequency of mice showing at least one meningeal metastasis along the surface of the brain is indicated below the diagram

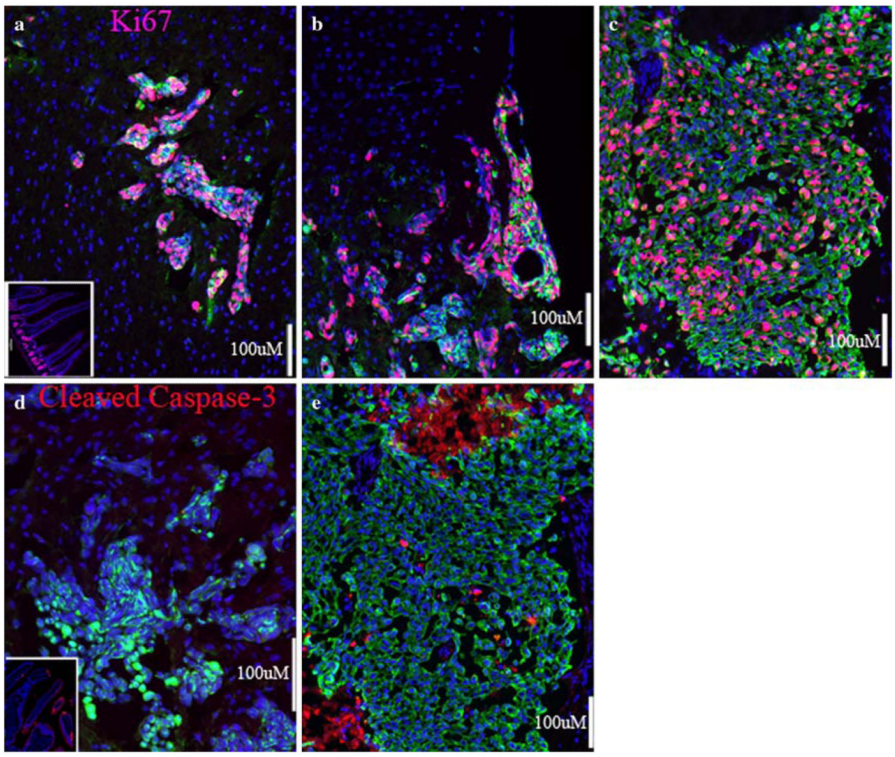

Fig. 3.

Life and death in breast cancer brain metastases. (**a**) A cluster of 231-BR cell metastases in the mouse cerebral cortex. Cycling cell nuclei, expressing Ki67, appear pink. Little to no proliferation is visible in the surrounding brain tissue. Inset in (**a**) shows positive-control staining with anti-Ki67 in the crypts of mouse intestine. (**b**) A meningeal metastasis at the surface of the brain shows levels of proliferation similar to that of parenchymal metastases. (**c**) A surgical sample from a brain metastasis of ductal carcinoma showing many Ki67-positive cycling tumor cells. (**d**) Apoptosis is rare in the xenograft model, as is apparent from the lack of staining for Cleaved Caspase-3 (red). Inset in (**d**) shows positive-control staining for Cleaved Caspase-3 in the villi of mouse intestine. (**e**) A few apoptotic cells are visible among the proliferating carcinoma cells from a surgical specimen of brain metastasis of ductal carcinoma. Necrotic areas, at the top and bottom left of (**e**) also show reactivity to the anti-Cleaved Capsase-3 antibody; (**c**) and (**e**) are from neighboring sections of the same metastasis. Five micron (human) or ten micron (mouse) sections were prepared from frozen samples and fixed with paraformaldehyde. Cytokeratin-positive tumor cells are stained green in all panels, and all nuclei counterstained with DAPI in blue. Scale bars indicate 100 micrometers

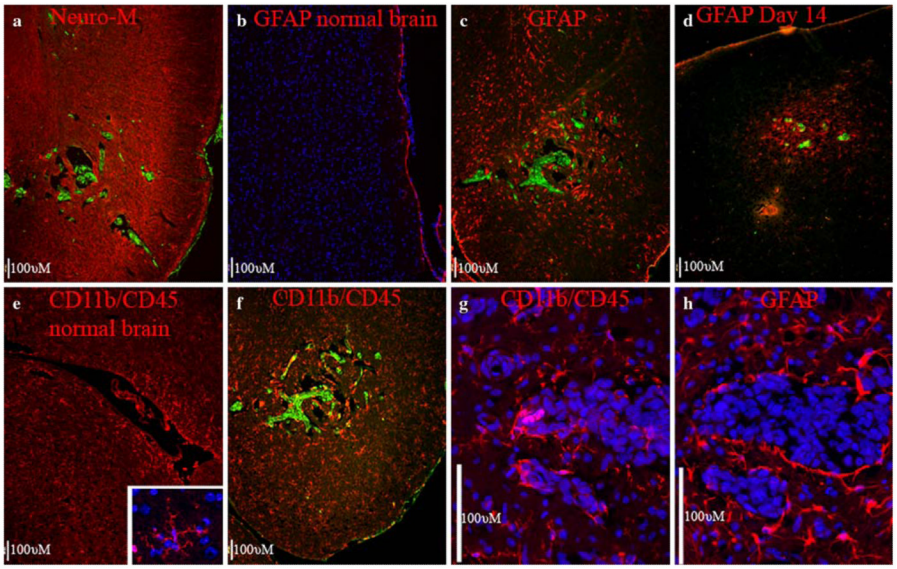

Fig. 4.

Interaction of 231-BR metastases with the mouse brain. (**a**) A cluster of metastases (green) separated from Neurofilament-M-positive neuronal cells (red) by edema. (**b**) Very few GFAP-positive astrocytes (red) are visible in the cerebral cortex of a control mouse brain. (**c**) One month after introduction of 231-BR brain metastatic cells, reactive astrocytes, visualized by staining for GFAP-positive cells, are visible in a large radius around the cluster of metastases. (**d**) Two weeks after introduction of 231-BR cells, only small metastases are apparent. GFAP-positive reactive astrocytes are already apparent at this early stage of colonization, and localize to the area of metastasis. (**e**) Resting microglia (red) in a normal mouse brain are weakly-positive for CD11b and CD45. Note increased staining around the ventricle. Inset shows a high magnification view of an arboreal microglial cell. (**f**) Reactive microglia also surround the metastases, visualized by increased staining for CD11b and CD45. (**g**) A cluster of metastases in the brain stem, showing a higher magnification view of CD11b and CD45 double-stained microglia/macrophages adjacent to the metastasis, as well as infiltrating the tumor mass. Nuclei are counterstained with DAPI (blue). The large, tightly-clustered nuclei correspond with cytokeratin-positive metastatic tumor cells. (**h**) A serial section through the same metastasis showing hypertrophic GFAP-positive astrocytes (red) in direct contact with metastatic cells along the tumor border. All panels are from ten micron cryostat sections fixed in paraformaldehyde. 231-BR cells are EGFP-positive, and stained with anti-cytokeratin (green in **a**, **c**, and **f**), or with anti-human mitochondria (green in **d**) and cell nuclei are stained with DAPI (blue in panels **b**, **g**, **h**, and the inset of **e**). Scale bars indicate 100 micrometers

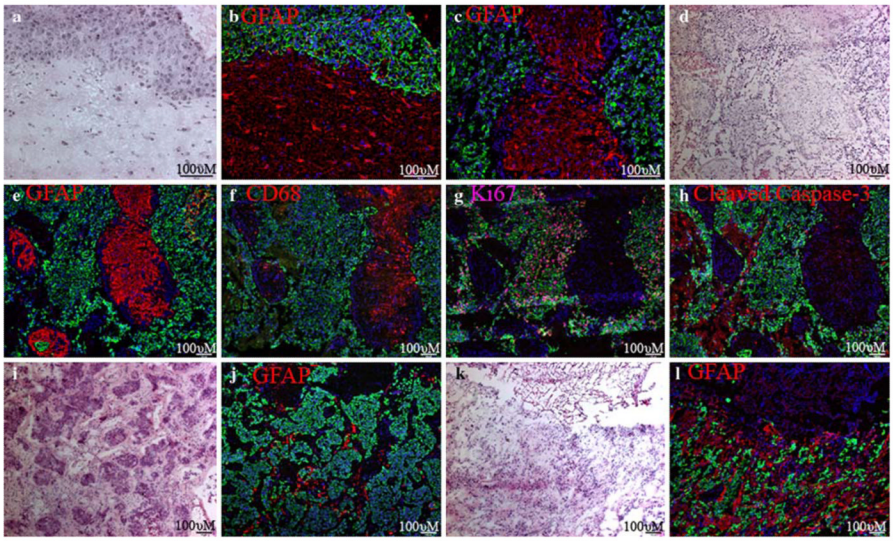

Fig. 5.

Large populations of glial cells are found in the inner tumor mass of surgically-resected brain metastases from breast cancer patients. (**a**) H&E stain along the border of a brain metastasis of infiltrating ductal breast cancer. (**b**) An anti-GFAP antibody (red) reveals astrocytes along the border of the metastasis shown in (**a**). (**c**) GFAP staining in the interior of a metastasis, showing an island of brain parenchyma trapped in the tumor. (**d-h**) Serial sections through the same metastasis of ductal breast cancer. (**d**) H&E stain in the interior of a metastasis. (**e**) Large islands of GFAP-positive astrocytes trapped between clusters of cytokeratin-positive carcinoma cells. (**f**) CD68-positive microglia/macrophages co-localize to the islands of astrocytes. (**g**) Ki67-positive nuclei are common amongst carcinoma cells, but rare in the trapped brain parenchyma. (**h**) Apoptotic cells, identified with an antibody to Cleaved Caspase-3, are found at a low frequency amongst carcinoma and brain parenchymal cells. Large necrotic areas are also visible by Caspase-3 staining. (**i**) H&E stain of another brain metastasis of ductal carcinoma with smaller clusters of metastatic tumor cells. (**j**) Ribbons of astrocytes are present between tumor cells of this metastasis. (**k**) H&E stain of a brain metastasis of lobular breast cancer. (**l**) “Indian files” of carcinoma cells in this metastasis are surrounded by many astrocytes. All panels are from five micron sections of snap-frozen tissue, post-fixed with paraformaldehyde. Carcinoma cells are labeled with anti-cytokeratin (green) and nuclei labeled with DAPI (blue) in panels **b**, **c**, **e-h**, **j** and **l**. Scale bars indicate 100 micrometers

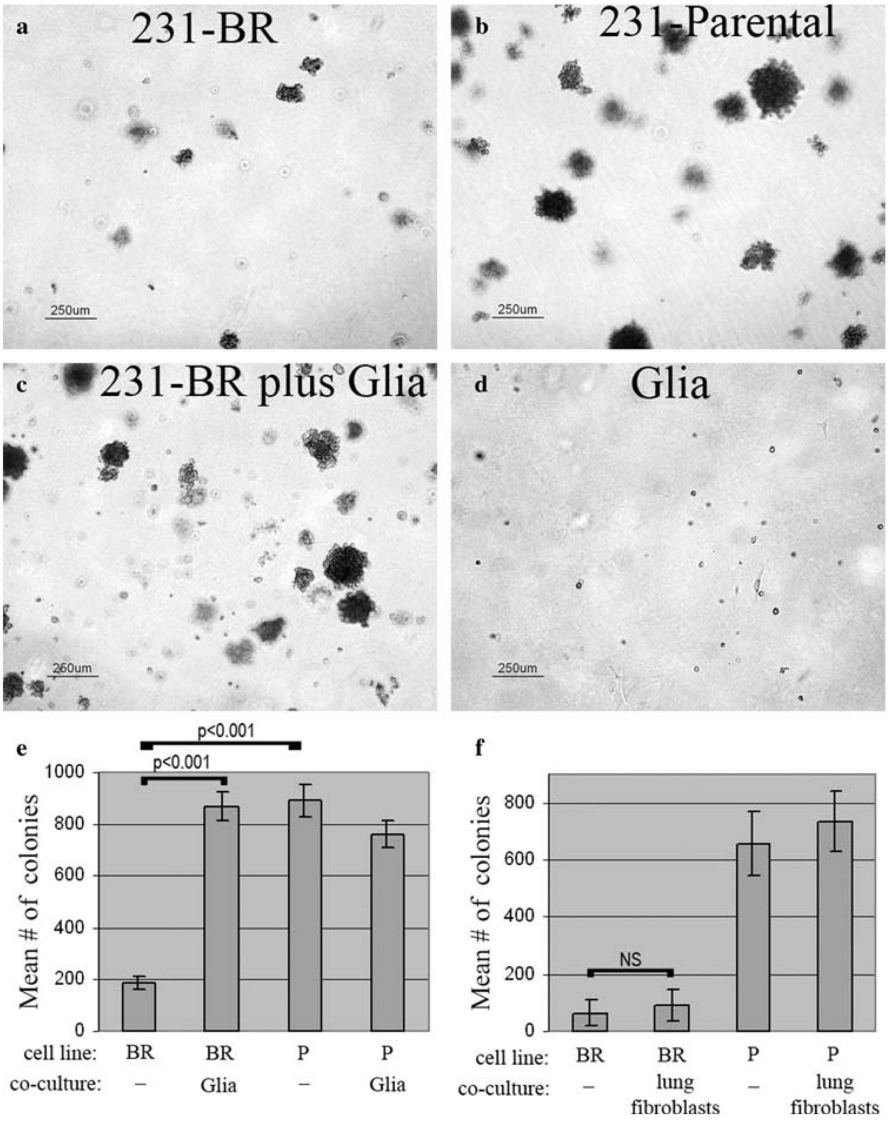

Fig. 6.

Glial cells from mouse cerebral cortex stimulate anchorage-independent growth of 231-BR cells in vitro. (**a**) Colonization by 231-BR cells alone for 14 days in soft agar. (**b**) Colonization by 231-Parental (lung metastatic) cells alone for 14 days in soft agar. (**c**) Increased colonization of 231-BR cells in co-culture with mixed glial cells for 14 days in soft agar. (**d**) Glial cells alone for 14 days in soft agar. (**e**) Quantification of a typical experiment, showing the effect of glia on 231-BR growth in soft agar. Mean number of colonies (>50 μm) from triplicate samples ± standard deviation are shown. Results of post-hoc Tukey-Kramer Multiple Comparisons Testing are shown on the graphs. BR = 231-BR (brain metastatic) cells; P = 231-Parental (lung metastatic) cells. (**f**) MRC-5 lung fibroblasts do not stimulate 231-BR cell growth in soft agar (NS = not significant)

Clin Exp Metastasis. Author manuscript; available in PMC 2009 May 8.

Table 1

Summary of immunofluorescence analysis of surgical brain metastasis specimens from breast cancer patients

Sample #	Age[a]	ER status[b]	Histologic classification[b]	TNM classification[b]	Proliferative index (%)[c]	Cell death[d]	Cytokeratin content[e]	Glial content[f]
1	36	-	Ductal	T_3N_1	53	+	+++	+++ (islands)
3	43	-	Ductal	$T_2N_0M_0$	50	+++	+++	++ (ribbons)
4	57	+	Ductal-lobular	$T_4N_0M_1$	39	++	++	++ (ribbons)
5	36	+	Ductal	$T_2N_{1a}M_1$	56	+	+	+ (at margins)
7	64	-	Ductal	T_1N_1	59	+	+++	+ (at margins)
11	66	-	Ductal	T_2	42	+++	+++	+++ (islands)
13[g]	68	-	Ductal	$T_1N_0M_0$	32	+	+++	-
14[g]	68	-	Ductal	$T_1N_0M_0$	41	+++	+++	+++ (islands)
15	50	-	Ductal with DCIS	$T_2N_0M_0$	61	+++	++	+
18	60	+	Ductal	$T_1N_0M_0$	57	No data	++++	-
21	60	-	Ductal	T_2N_0	28	+++	+++	+++ (islands)
22	54	-	Lobular	$T_{1c}N_2$	9	++	+++	++++ (ribbons)
23	58	+	Lobular	T_2N_2	24	+	++++	++ (ribbons)
24	58	-	Inflammatory	$T_{1c}N_x$	50	+++	++ (discrete clusters)	++++
25[h]	61	-	Ductal	$T_2N_1M_0$	48	+++	+++	+++ (islands)
26[h]	61	-	Ductal	$T_2N_1M_0$	48	+++	+++	+++ (islands)

[a] Age of patient at time of diagnosis of brain metastasis

[b] Classification of the primary tumor (ER = estrogen receptor)

[c] Percentage of Ki67-positive cells among Cytokeratin-positive metastatic cells (>150 cell nuclei counted per sample)

[d] Amount of Cleaved (Active)-Caspase-3 staining in metastatic brain tumors, includes areas of necrosis (scale of 1 to 3^+, $^{+++}$ indicates extensive necrosis)

[e] Amount of Cytokeratin-positive staining in metastatic brain tumors (anti-Cytokeratin MNF116, scale of 1 to 4^+)

[f] Amount of GFAP-positive astrocyte staining in metastatic brain tumors (scale of 0 to 4^+)

[g] Individual brain metastases removed from the same patient

[h] Individual brain metastases removed from the same patient